



1 Modeling of GPS total electron content over the African low latitude 2 region using empirical orthogonal functions

3 Geoffrey Andima^{a,*}, Emirant B Amabayo^{a,b}, Edward Jurua^a, Pierre J Cilliers^c

4 ^a*Department of Physics, Mbarara University of Science and Technology, Mbarara, Uganda*

5 ^b*Department of Physics, Busitema University, Tororo, Uganda*

6 ^c*South African National Space Agency (SANSA) Space Science, Hermanus, South Africa*

7 Abstract

In this paper, an empirical total electron content (TEC) model and trends in TEC over the African low latitude region are presented. GPS-derived TEC data from Malindi, Kenya (geographic coordinates 40.194°E, 2.996°S) and global ionospheric maps (GIMs) were used. We employed empirical orthogonal function (EOF) analysis method together with least square regression to model the TEC. The EOF-based TEC model was validated through comparisons with GIMs, GPS-derived TEC and TEC derived from the International Reference Ionosphere-2016 (IRI-2016) model for selected quiet and storm conditions. The single station EOF-based TEC model over Malindi satisfactorily reproduced the known diurnal, semiannual and annual variations in the TEC. Comparison of the EOF-based TEC model results with TEC derived from IRI-2016 model showed that the EOF-based model predicted the TEC over Malindi with less errors than the IRI-2016. For the selected storms, the EOF-based TEC model simulated the storm time TEC response over Malindi better than the IRI-2016. In the case of the regional model, the EOF-based TEC model was able to reproduce the TEC characteristics in the equatorial ionization anomaly region. The EOF-based TEC model was then used as a background in estimating TEC trends. A latitudinal dependence in the trends was observed over the African low latitude region.

8 *Key words:* TEC model, Empirical orthogonal functions, TEC Trends

9 1. Introduction

10 The features of the low latitude ionosphere are quite unique. During daytime, a double peaked
11 ionization structure appears over the low latitude region, a phenomenon often referred to as
12 the equatorial ionization anomaly (EIA). The EIA is normally explained in terms of the plasma
13 fountain theory (Martyn, 1947; Moffett, 1979). The daytime E region eastward electric field
14 in combination with the nearly horizontal Earth's magnetic field generate a large vertically
15 directed $E \times B$ drift force at the dip equator that raises the plasma to higher altitudes. The
16 raised plasma diffuses away from the geomagnetic equator under gravity and pressure gradient
17 forces along the equipotential magnetic field lines to form ionization peaks at dip latitudes
18 $\sim \pm 15^\circ$, and a trough that extends over the dip equator (Appleton, 1946). Prior to the electric
19 field turning westwards at night, it is enhanced (prereversal enhancement (PRE)) resulting
20 in plasma uplift into regions of low recombination. Associated with the electron density at
21 the EIA enhancement is a density gradient instability of the Rayleigh Taylor (RT) type which
22 creates a spectrum of plasma irregularities that fill the post sunset low latitude ionosphere
23 (Kelley, 2009). The EIA and the PRE vary with location, solar activity, season, and even on
24 daily basis. These variations make it difficult to predict the characteristics of the low latitude
25 ionosphere.

*Corresponding author

Email address: geoffrey.andima@gmail.com (Geoffrey Andima)

Preprint submitted to *Annales Geophysicae*



1 The state of the ionosphere is of great importance in space based navigation systems such
2 as the Global Navigation Satellite Systems (GNSS). The total electron content (TEC) is of
3 particular interest to users of GNSS systems. For many practical purposes in the GPS, the
4 desired ionospheric parameter is the TEC. This is because many of the effects on transiono-
5 spheric satellite links (e.g time delay, Polarization, Faraday rotation, Doppler shift) are related
6 to TEC in one way or another (Kersley et al., 2004). The low latitude ionosphere exhibits
7 the highest values of TEC globally. Therefore, pronounced ionospheric effects are experienced
8 by radio signals transiting the low latitude ionosphere. Understanding the low latitude iono-
9 spheric dynamics in a bid to forecast its day to day conditions is key for advancement of space
10 technology and the improvement of GNSS accuracy.

11 Ionospheric variability over the low latitude region of Africa, based on TEC analysis, has
12 been reported before (e.g Adewale et al. 2011; Olwendo et al. 2012; Habarulema et al. 2013;
13 Andima et al. 2015). From these studies, the diurnal, seasonal, disturbed and quiet time TEC
14 characteristics over the region have been revealed. However, these analyses made use of TEC
15 data of either the same solar phase or the same solar cycle. With now a relatively longer
16 record of data in the achieves, it is imperative to extend these studies to the long-term TEC
17 characteristics over the African low latitude region for practical applications.

18 A common approach to TEC prediction is through modeling. Various TEC models (e.g
19 Anderson et al. 1987; Rawer and Bilitza 1990; Reinisch et al. 2004; Lean et al. 2011; Hajra
20 et al. 2016; Ercha et al. 2012; Chen et al. 2015; Ercha et al. 2012) have been developed;
21 however, many of these models are limited in geographical extend. A widely used model to
22 describe the global TEC climatology is the International Reference Ionosphere (IRI) model
23 (Bilitza, 1990). The IRI is an empirical model synthesized from global data sets comprising of
24 ionosonde, radar and in situ measurements (Bilitza, 1990; Rawer and Bilitza, 1990). Averaging
25 and smoothing applied when deriving the model coefficients may limit its accuracy in capturing
26 peculiar features such as the TEC variability in the EIA region. Under such circumstances,
27 regional models are superior in characterizing the background TEC.

28 Long term trends in ionospheric parameters are indicative of the deviation in the ionospheric
29 parameters from their background values. Ionospheric trends are important in understanding
30 the changes in Earth's energy balance (Elias, 2011). Various studies (e.g Jarvis et al. 1998;
31 Bencze 2002, 2005; Lastovicka et al. 2006; Danilov and Mikhailov 1999; Bremer et al. 2012)
32 have reported on long-term trends in ionospheric parameters derived from ionosonde data.
33 A conclusion from these studies is that trends in the F2 layer critical frequency (foF2) and
34 F2 layer maximum electron density height (hmF2) are negative. Some studies on ionospheric
35 trends have also revealed latitudinal dependence of these trends (Danilov and Mikhailov, 1999).
36 Lean et al. (2011) using a database of global ionospheric maps (GIMs) reported that global
37 TEC trends are positive and are dependent on the geomagnetic latitude. Also cases of negligible
38 or no trends in TEC have been observed. For instance, results obtained by Lastovicka et al.
39 (2017) show a weak negative or no trend in ionospheric TEC. Despite the various studies on
40 trends of different ionospheric parameters, those relating to TEC remain limited, and hence
41 the question on the nature of ionospheric TEC trends still need to be answered. There is a
42 need to investigate whether TEC has negative (Lastovicka et al., 2017), or positive (Lean et al.,
43 2011), or no (Lastovicka, 2013) trend. The objective of this paper is therefore two fold: first
44 to attempt to model low latitude TEC and secondly to estimate trends in the variation of
45 the ionospheric TEC over the African low latitude region using actual TEC measurements by
46 means of regional GPS receivers, and data from the GIMs.

47 2. Data sets used

48 The International GNSS Service (IGS) operates a number of GPS ground based receivers over
49 the African low latitude region. In this study, data was obtained from one of the IGS receivers



1 located at Malindi, Kenya which archived data from 1995 to date (December 2017). Prior
 2 to 2008, the IGS receiver (station code MALI) was installed at 40.19439° E, 2.99591°S and
 3 then replaced with another (station code MAL2) installed at 40.19414°E, 2.99606°S. These
 4 receivers had nearly the same location and therefore sampled the same geographical region of
 5 the ionosphere. We obtained the Receiver Independent EXchange (RINEX) files from `ftp://`
 6 `cddis.gsfc.nasa.gov/` and then extracted the TEC along the line-of-site, slant TEC (sTEC),
 7 from the RINEX files using the GPS-TEC software of Boston College (Seemala and Valladares,
 8 2011). This software uses the thin shell mapping function to map the sTEC to the vertical
 9 to obtain the vertical TEC (vTEC) at an assumed ionospheric height of 350 km. The vTEC
 10 for the different viewing geometries for satellites with elevation angles greater than 30° were
 11 averaged epoch-by-epoch to give a representation of the vTEC above the receiver. Due to
 12 data paucity from 1995 to 1998, only data from 1999 to 2017 were used in this study. Hourly
 13 averages of the daily TEC data were then calculated to minimize noise in the data. The hourly
 14 averages were organized into a data matrix $M_{d \times h}$ (day×hour) which was used to model and
 15 estimate trends in TEC over Malindi. To study the TEC over the African low latitude region,
 16 TEC from the GIMs, a reliable source of ionospheric data (Hernandez-Pajares et al., 2009), was
 17 used. Though these maps have been available since 1998, for comparison purposes with the
 18 GPS data, we have used data from 1999-2017. It is worthy noting that the two hourly GIMs
 19 were interpolated to hourly data.

20 3. Single station model over Malindi

21 3.1. EOF decomposition of the TEC data

22 Empirical orthogonal function (EOF) analysis is a well-known method that dates back to the
 23 work of Pearson (1901), and has been widely used in climate (Hannachi et al., 2007) and
 24 ionospheric (Dvinskikh, 1988; Zhang et al., 2009; Liu et al., 2008) data analysis. It involves
 25 reducing the dimensionality of the data by finding a set of few variables (EOF modes or basis
 26 vectors) that explain most of the variability in the data. This allows for the original data
 27 (TEC(d, h)) to be expressed as a linear combination of the few basis functions as

$$28 \quad \text{TEC}(d, h) = \sum_{j=1}^n U_j(h) \times C_j(d), \quad (1)$$

29 where C_j is the coefficient of the basis vector $U_j(h)$ with the index j running from 1 to n (the
 30 number of the retained EOF modes). We used the method of singular value decomposition
 31 (svd) to determine the EOF modes that explain most of the variability in the TEC data. The
 32 TEC data matrix M was decomposed into U and V , the left and right basis vectors respectively,
 and S a matrix of singular values of M according to the equation

$$33 \quad M = USV^T \quad (2)$$

34 The first six EOF modes in matrix U and their corresponding coefficients obtained using
 35 equation 3 are shown in Figure 1. While Table 1 shows the percentage variability in the data
 explained by the different EOF modes.

$$36 \quad C_j(d) = S \times V_j^T \quad (3)$$

37 Figure 1 (a) shows that the average diurnal TEC over MAL2 has a maximum value at about
 38 11:00 UT and a secondary maximum at about 20:00 UT. The daytime peak at 11:00 UT
 39 is possibly due to increased ionization as the solar zenith angle is nearly zero over Malindi
 around this time. The secondary maximum could be due to an enhancement in the eastward

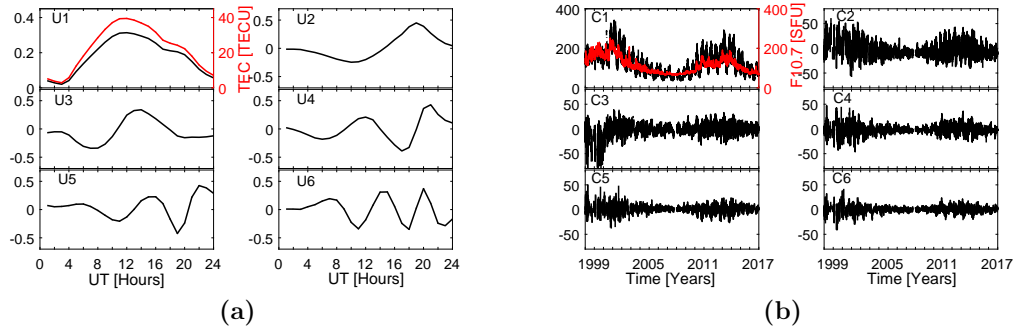


Figure 1: The first six basis functions (a) representing the diurnal variation and their coefficients (b) which show the long-term variation of TEC over MAL2

Table 1: Variance of the TEC data explained by the different EOF modes

EOF mode	1	2	3	4	5	6
Explained Var.	96.8	1.0	0.8	0.3	0.20	0.1
Cumulative	96.8	97.8	98.6	98.9	99.1	99.2

1 electric field before its westward reversal at night. Though the physical interpretation of the
 2 basis functions are normally difficult due to their geometric nature (Hannachi et al., 2007),
 3 the high correlation between the first basis mode U1 with the mean TEC shows that U1 is
 4 replicating the diurnal characteristics of the ionospheric TEC over Malindi. The fluctuations
 5 observed in the higher order basis functions could be signatures of the different processes
 6 (such as traveling thermospheric disturbances (TADs)) that influence the low latitude plasma
 7 dynamics. Figure 1 (b) shows that the semiannual and annual variations in TEC have peaks
 8 during the equinoxes and high solar activity years respectively. These coefficients are well
 9 correlated with the solar radio flux measured at 10.7 cm wavelength (F10.7), confirming that
 10 the main driver of ionospheric variability over Malindi is the changes in the extreme ultraviolet
 11 (EUV) radiation from which the ionosphere owes its existence.

12 3.2. Modeling of the coefficients

13 Due to the rapid convergence of the basis functions, we used only the first six EOF modes
 14 which accounted for 99.2% of the explained variance in the data to model the observed regional
 15 TEC as derived from GNSS measurements at Malindi. The coefficients were modeled in terms
 16 of harmonic functions with periods of 0, 0.5 and 1 year to represent the linear, semiannual and
 17 annual variations respectively using equations 5–7.

$$C_j(d) = B_{j1}(d) + B_{j2}(d) + B_{j3}(d) \quad (4)$$

18 where

$$B_{j1}(d) = a_{j1} + b_{j1}F10.7(d) + c_{j1}Dst(d) \quad (5)$$

19

$$B_{j2}(d) = [a_{j2} + b_{j2}F10.7_{av}(d) + c_{j2}Dst(d)] \cos\left(\frac{2\pi d}{365.25}\right) + [d_{j2} + e_{j2}F10.7_{av}(d) + f_{j2}Dst(d)] \sin\left(\frac{2\pi d}{365.25}\right) \quad (6)$$

20

$$B_{j3}(d) = [a_{j3} + b_{j3}F10.7_{av}(d) + c_{j3}Dst(d)] \cos\left(\frac{4\pi d}{365.25}\right) + [d_{j3} + e_{j3}F10.7_{av}(d) + f_{j3}Dst(d)] \sin\left(\frac{4\pi d}{365.25}\right) \quad (7)$$



1 The daily averaged disturbance storm-time (Dst) and F10.7 indices used in the modeling process
2 were downloaded from Omniweb¹. The F10.7_{av} used in equations 5–7 was calculated from
3 $F10.7_{av} = \frac{1}{2}(F10.7 + F10.7_{81})$, where F10.7₈₁ was the 81 day running average of F10.7. After
4 estimating the coefficients using a least squares fit to the GPS-derived TEC values measured
5 at Malindi, the modeled TEC was obtained using equation 1 by replacing the coefficients with
6 their modeled values. The variation of the observed GPS-derived TEC, the reconstructed TEC
7 from the first six EOF modes, and the modeled TEC are shown in Figure 2. It can be seen from
8 Figure 2 a & b that the six EOF modes were sufficient to reproduce the variation in the TEC.
9 Figure 2 c shows that the model quite well captured the diurnal, seasonal and the solar activity
10 variations in the observed TEC over Malindi. Correlation analysis between the observed and
11 the modeled TEC show a high positive correlation (Figure 2 d) with a correlation coefficient of
12 0.9225. This high correlation is an indication of the EOF decomposition method being capable
13 of reproducing the inherent features of the dynamic ionosphere at the crest of the anomaly
region.

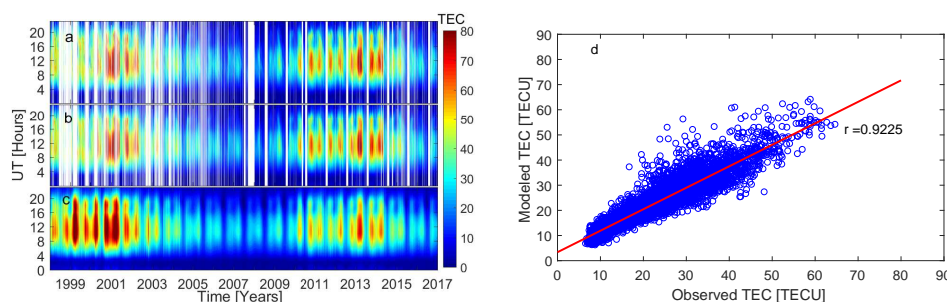


Figure 2: (a) GPS TEC, (b) reconstructed TEC and (c) modeled TEC over Malindi. (d) Correlation between EOF modeled TEC and GPS-derived TEC over Malindi from 1999 to 2017

14

15 3.3. Model validation

16 To assess the performance of the EOF-based TEC model, we compared the model results with
17 the TEC derived from IRI-2016 model and GIMs obtained from the website² of Center for Orbit
18 Determination in Europe (CODE). From here onwards, TEC from the EOF-based TEC model
19 will be referred to as EOF TEC, TEC derived from the GPS receiver in Malindi as GPS TEC,
20 TEC from CODE's GIMs as CODE's TEC and TEC from IRI-2016 model as IRI TEC. We
21 used both Kp and Dst to characterize the days into quiet and disturbed. A day was considered
22 to be quiet if $Kp \leq 3$.

23 3.3.1. Quiet days

24 Quiet days were selected from the equinox (March and September) and solstice (June and
25 December) months of high (2002), low (2009) and ascending (2011) solar activity phases in order
26 to validate the EOF-based TEC model. The data for the selected quiet days were excluded
27 from the matrix used to generate the model coefficients, and the same procedure for model
28 construction was repeated. The IRI TEC for the selected days were obtained from the web
29 interface of IRI-2016 model hosted at Omniweb³. To retrieve the IRI TEC, the location was
30 specified to coincide with the geographic coordinates of MAL2 GPS receiver and the topside

¹<https://omniweb.gsfc.nasa.gov/>

²<ftp://ftp.aiub.unibe.ch/CODE/>

³https://omniweb.gsfc.nasa.gov/vitmo/iri2016_vitmo.html



1 boundary was set to its maximum value of 2000 km. The NeQuick option was used as the topside
 2 electron density model and ABT-2009 for the bottom side thickness. Figure 3 shows hourly
 3 diurnal variation of GPS TEC, IRI TEC, EOF TEC and CODE's TEC over Malindi for some
 selected quiet days. As expected, TEC values were higher in 2002, followed by 2011 and then

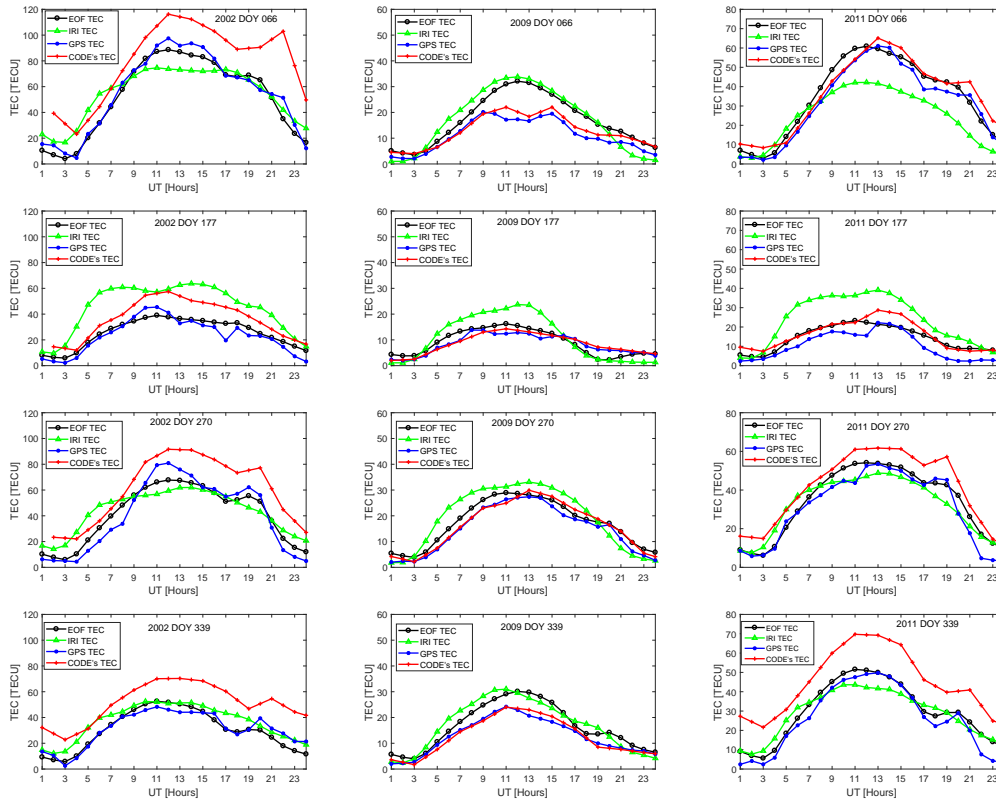


Figure 3: GPS TEC, IRI TEC, CODE's TEC and the EOF TEC over Malindi for some selected quiet days

4
 5 2009. The IRI-2016 model overestimated the diurnal TEC over Malindi during the low solar
 6 activity year 2009 and during winter solstice of all the years. The overestimate of the GPS TEC
 7 by the IRI TEC is similar to what Olwendo et al. (2012) observed when they compared GPS
 8 TEC measurements over Kenya with TEC from IRI-2007 model. During the equinox months of
 9 higher solar activity years, IRI TEC values were higher and lower than the GPS TEC at about
 10 3:00-9:00 UT and 11:00-13:00 UT respectively. The CODE's TEC overestimated the GPS TEC
 11 especially during the higher solar activity years 2002 and 2011. The overestimate of the GPS
 12 TEC by CODE's TEC was not much reflected during the low solar activity year 2009. The
 13 EOF TEC on the other hand replicated the diurnal TEC quite well except on day of the year
 14 (DOY) 066 and DOY 339 in 2009. In general, the highest correlation was observed between the
 15 GPS TEC and CODE's TEC followed by the correlation of the GPS TEC with the EOF TEC.
 16 It is worth noting that CODE's TEC mainly overestimated the TEC over Malindi especially
 17 during higher solar activity years. Meanwhile, the IRI-2016 overestimated the GPS TEC over
 18 MAL2 between 03:00 and 07:00 UT during high solar activity periods, and throughout the day
 19 during lower solar activity years. This may be due to inadequate ingestion of ground based
 20 data from the East African region in to the IRI model. As earlier mentioned, measurements



1 from ionosondes were used to provide ground data during IRI model construction, and such
 2 data is currently limited over East Africa.

3 3.3.2. Disturbed days

4 To study the storm time performance of the EOF-based TEC model, we simulated TEC for
 5 some selected geomagnetic storms. As stated earlier, the test days were excluded in the process
 6 of generating the model coefficients. The IRI TEC for the storm days were obtained with
 7 the storm model turned on. Figure 4 shows variation of the hourly diurnal TEC during some
 selected major geomagnetic storms. In Figure 4 a, TEC variation for a storm that occurred

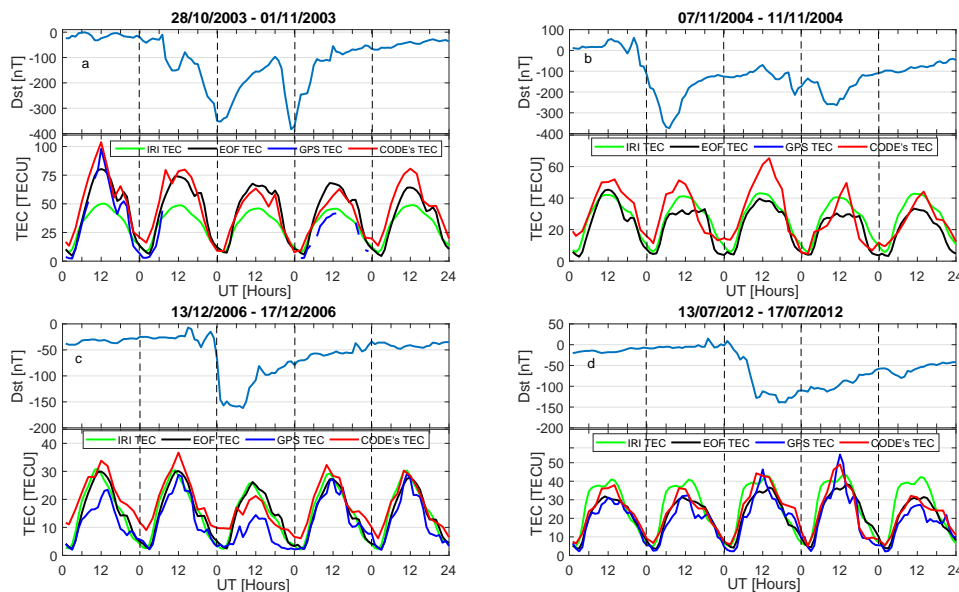


Figure 4: GPS TEC, IRI TEC, CODE's TEC and EOF TEC over Malindi for some selected storms. In these plots, the GPS TEC values are taken as a true representation of the ionosphere over Malindi. However, in the absence of GPS TEC, CODE's TEC were used to describe the ionospheric response to the storms

8
 9 from 29-30 October 2003 are shown. No continuous GPS TEC measurements were available
 10 from MAL2 IGS receiver during this storm period. As can be seen in CODE's TEC, the
 11 storm had negative effect on the peak value of the TEC. The same negative storm effect was
 12 replicated by the EOF and IRI models especially on 30-31 October 2003. Another major storm
 13 occurred from 08-10 November 2004 with the main phase on the 08 November 2004 (Figure 4
 14 b). Similarly, during this period, GPS TEC measurements were not available from MAL2 IGS
 15 receiver. Both CODE's TEC and EOF TEC revealed negative storm effects on 08-November
 16 and 10-November 2004 (Figure 4 b). However, the IRI TEC was not sensitive to the effect of the
 17 geomagnetic storm. In Figure 4 c, the EOF TEC, CODE's TEC and IRI TEC showed negative
 18 storm effects, consistent with the GPS TEC during the storm that occurred on 15-December
 19 2006. A case of positive storm time effect on the ionosphere is shown in Figure 4 d where the
 20 EOF TEC and CODE's TEC showed similar positive storm time effect as in the GPS TEC.
 21 This was not reflected in the TEC derived from the IRI-2016 model.

22 3.3.3. Statistical analysis

23 From the EOF-based TEC model, we have simulated TEC for the months of March, June,
 24 September and December for low (2009) and high (2013) solar activity years. In each of these



1 simulations, the data for the selected months were excluded from the data used to generate
 2 the model coefficients. It is worthy noting that in generating the model coefficients, say for
 3 March 2009, it is only the data of March 2009 that was excluded. The monthly median values
 4 for the EOF TEC, IRI TEC and CODE's TEC were used to compute the root mean square
 5 error (rmse) of the predicted TEC from the GPS TEC for every hour of the day. The diurnal
 variation of the rmse values in 2009 and 2013 are shown in Figure 5. From Figure 5, the

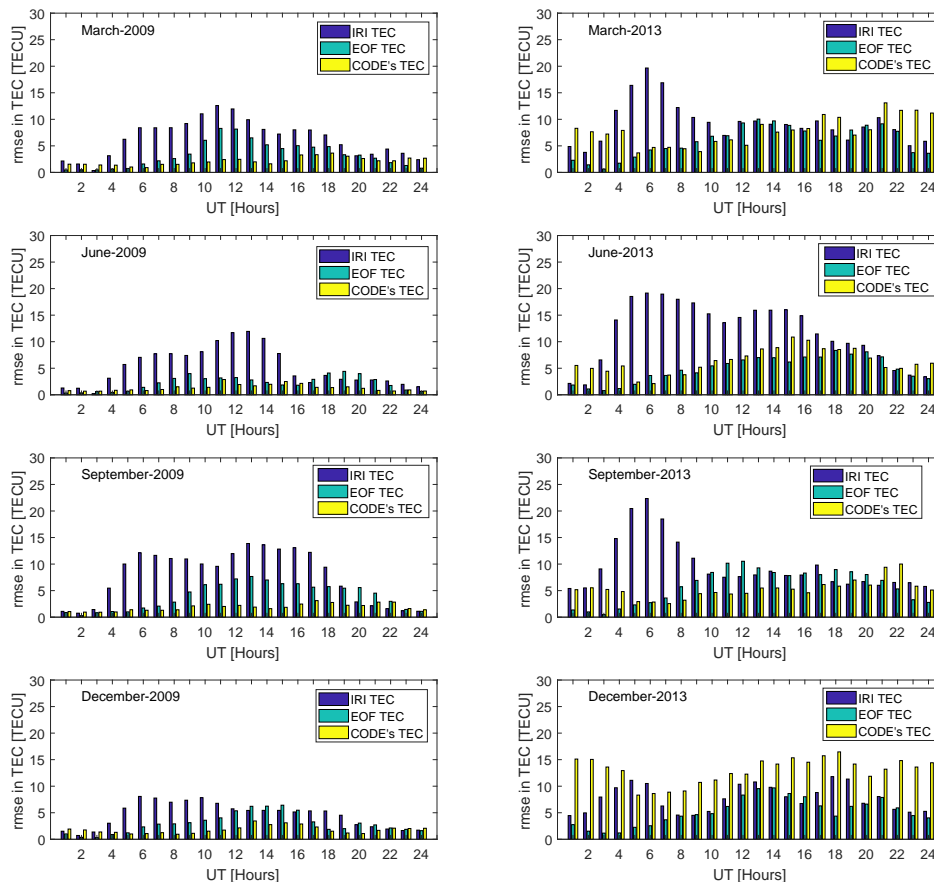


Figure 5: Diurnal variation of root mean square error (rmse) of IRI TEC, CODE's TEC and EOF TEC relative to GPS TEC over Malindi

6
 7 uncertainty in predicting the observed TEC was higher in 2013 than in 2009. This could be
 8 due to intensification of equatorial electrodynamic processes and the associated effects such as
 9 TEC perturbations during higher solar activity years (Andima et al., 2015). These secondary
 10 effects of the equatorial dynamo processes are not probably well captured by the models. A
 11 comparison of the performance of the different models has shown that, CODE's GIMs predicted
 12 the TEC over MAL2 with the least rmse values followed by the EOF model in 2009. The
 13 greatest uncertainty in predicting the TEC over MAL2 in the same year was observed in the
 14 IRI-2016 TEC. Similarly in 2013, the IRI TEC had higher rmse values compared to the EOF
 15 TEC. CODE's GIMs showed the largest uncertainty in predicting the TEC over MAL2 during
 16 December solstice of the high solar activity year 2013. The diurnal uncertainties in the ability
 17 of IRI-2016 to predict the TEC over MAL2 exhibited two peaks in March, June and September



1 in 2009. The maximum rmse values in the IRI-2016 predicted TEC were observed between
 2 11:00 and 13:00 UT in March and June, and 13:00-14:00 UT in September in 2009. December
 3 solstice showed a single peak in the rmse values from 06:00-7:00 UT in 2009. Both the EOF
 4 TEC and CODE's TEC had the largest rmse values from 11:00-14:00 UT in the same year. The
 5 rmse values from 16:00-18:00 UT in March and September 2009 were quite higher than those
 6 in June and December of the same year. In 2013, the rmse in the IRI-2016 predicted TEC in
 7 the months of March and September had only single peaks which occurred at about 06:00 UT.
 8 However, two peaks, one between 04:00 and 07:00 UT and second between 13:00 and 14:00 UT
 9 were observed in June and December 2013. The smallest error in the IRI TEC and the EOF
 10 TEC were observed after local midnight to about 03:00 UT in both 2009 and 2013.

11 4. Modeling TEC over African low latitudes

12 The first step in the regional TEC modeling was to extract the TEC for the African low
 13 latitude region from CODE's GIMs. The daily GIMs were organized into bins of $2.5^{\circ} \times 5^{\circ} \times 1$ Hr
 14 (latitude \times longitude \times LT). The binned data was then decomposed into the spatial and temporal
 15 components according to the equation

$$16 \quad \text{TEC}(\text{lat}, \text{lon}, \text{LT}, m) = \sum_{i=1}^r U_i(\text{lon}, \text{lat}) \times P_i(\text{LT}, m) \quad (8)$$

16 In equation 8, $U_i(\text{lon}, \text{lat})$ are the basis modes representing the spatial TEC variability and
 17 $P_i(\text{LT}, m)$ are the coefficients that describe the temporal TEC variations in terms of local time
 18 (LT) and month (m). Figure 6 (a) shows the first four basis modes from the decomposition
 in equation 8, and their corresponding expansion coefficients are shown in Figure 6 (b). The

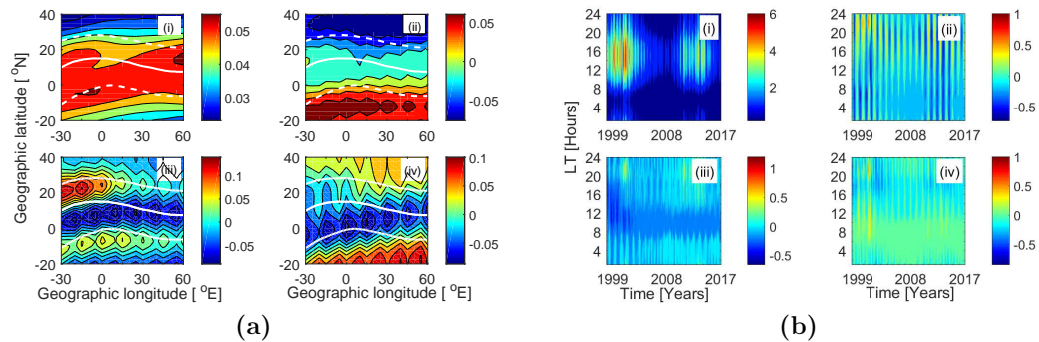


Figure 6: (a) The first four basis vectors from the first layer decomposition of the TEC data. (b) The coefficients of the basis modes in (a)

19 first basis mode (Figure 6 (a) (i)) replicated the average TEC over African low latitude region
 20 for the period 1999-2017, and therefore represents the average TEC characteristics over Africa.
 21 This mode accounts for 97.012% of the TEC variability over the region. The coefficients of the
 22 first basis mode show that TEC over African low latitudes exhibits, diurnal, seasonal and solar
 23 activity dependences (Figure 6 (b) (i)). Shown in Figure 6 (a) (ii) is the second basis mode and
 24 the coefficients of this mode are shown in Figure 6 (b) (ii). The second basis mode accounts
 25 for 1.255% of the total TEC variability and it demonstrates the TEC variability in the two
 26 hemispheres, possibly due to differences in the seasons in the two hemispheres. In Figure 6
 27 (a) (iii), the effect of the magnetic and electric field coupling resulting in the EIA appears to
 28 be evident. This mode accounts for 0.455% of the total TEC variability over the African low
 29 latitude region.
 30



1 The temporal component in equation 8 was further broken into the diurnal and long-term
 2 (seasonal, annual and solar cycle) variations by another decomposition which we refer to here
 3 as the second layer decomposition expressed as

$$P_i(LT, d) = \sum_{i,j=1}^m U_{i,j}(LT) \times A_{i,j}(d). \quad (9)$$

4 In equation 9, $U_{i,j}(LT)$ are the basis functions of the i^{th} first level coefficients and $A_{i,j}(d)$
 5 are the coefficients of $U_{i,j}(LT)$. Figure 7 (a) show the first basis modes for each of the first
 four expansion coefficients in the first level decomposition. Equations 5 - 7 were then used to

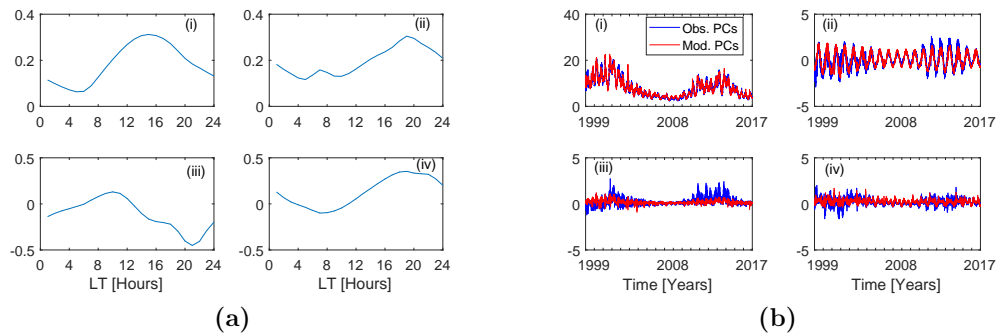


Figure 7: (a) The first basis modes of the first four first layer expansion coefficients. (b) The expansion coefficients (blue) and their modeled values (red) for the basis modes in (a).

6
 7 model the coefficients $A_{i,j}(d)$. Figure 7 (b) shows the coefficients $A_{i,j}(d)$ together with their
 8 model predicted values. Using the modeled values of the coefficients, the regional TEC was
 9 then reconstructed in a reverse order. We first used equation 9 to obtain the coefficients for
 10 the first layer decomposition and then applied equation 8 to determine the TEC in each grid
 11 cell. Figure 8 shows the modeled TEC, CODE's TEC and IRI TEC for DOY 070 in 2015. It
 12 can be seen from Figure 8 that the model has quite well reproduced the main features of the
 13 EIA region. Higher correlations are observed between EOF modeled TEC and CODE's TEC
 14 (Figures 8 a & b). This high correlation is an indication that the model predicted results could
 15 offer a good alternative in estimating background TEC since CODE's TEC are derived from
 GNSS measurements.

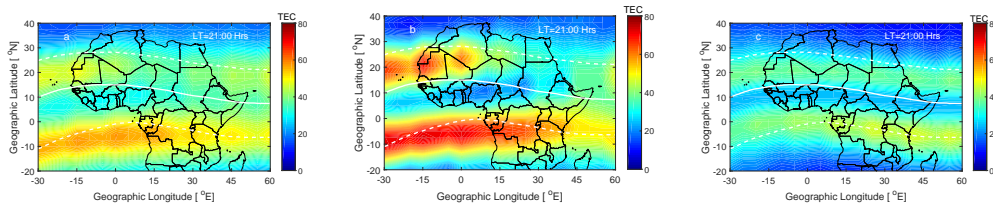


Figure 8: EOF TEC (a), CODE's TEC (b) and the IRI TEC (c) for the DOY 070 in 2015. Shown on the plots are the local times in hours

16

17 5. TEC trends

18 In the past, few studies (e.g Lean et al. 2011; Lastovicka et al. 2017) have derived long-term TEC
 19 trends, and these mainly used TEC data from GIMs. In this work, we have used GPS-derived



1 TEC and GIMs to study TEC trends over the low latitude region of Africa. A key aspect
 2 in trend studies is the art of suppressing the solar and magnetic activity influences on these
 3 trends. We used the EOF modeled TEC as background TEC to remove the solar and magnetic
 4 effects in influencing the TEC trends. First, the monthly median TEC values were calculated
 5 from the daily TEC. The median TEC values were then modeled using similar equations as in
 6 equations 5–7. In these equations, the daily inputs were replaced with their monthly averages.
 7 The modeled TEC values were then subtracted from the monthly medians to obtain the TEC
 8 residuals (ΔTEC). The trend was then determined using the equation (Lastovicka et al., 2006;
 9 Bremer et al., 2012).

$$\Delta\text{TEC} = A + B \cdot \text{time (year)} \quad (10)$$

10 where A is the constant part and B the slope (trend) of the time-dependent TEC residuals.
 11 Lastovicka et al. (2017) attributed the positive global TEC trends reported in Lean et al.
 12 (2011) to lower TEC values in CODE’s GIMs especially prior to 2003. To test this assertion,
 13 we have estimated the long-term trends in TEC for the periods 1999-2017 and 2003-2017
 using GPS-derived TEC, CODE’s TEC and TEC from IGS GIMs. Figure 9 shows the TEC

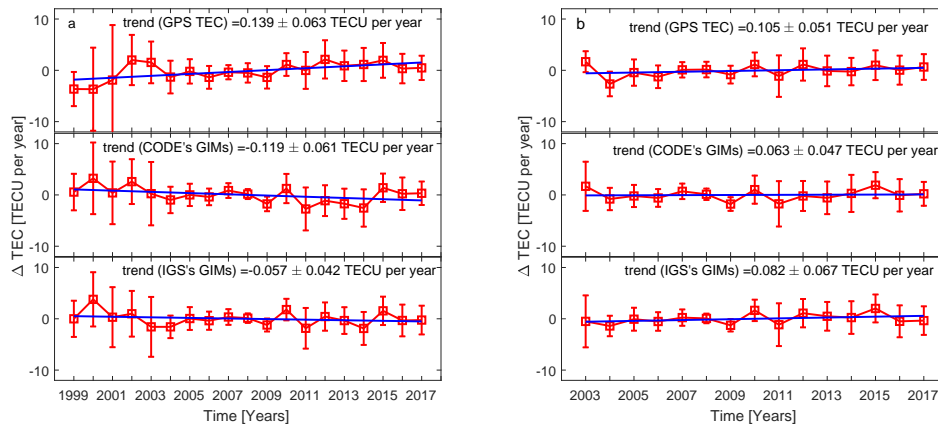


Figure 9: The yearly median residual TEC after removing the solar and magnetic activity variations for the periods 1999-2017 (a) and 2003-2017 (b). The upper panels are for the TEC derived from MAL2 IGS receiver, the middle panels are for TEC from CODE’s GIMs and the lower panels are for TEC from IGS’s GIMs corresponding to the location of MAL2 IGS receiver. The straight lines in these plots are the first degree polynomial fits used to estimate the trends

14 trends obtained from GPS-derived TEC and TEC from GIMs of CODE and IGS over Malindi.
 15 Trends of 0.139 ± 0.063 TECU/year, -0.119 ± 0.061 TECU/year and -0.057 ± 0.042 TECU/year
 16 were obtained using the GPS TEC, CODE’s GIMs and IGS GIMs over Malindi respectively.
 17 Though the trend values in Figure 9a were slightly different, their 95% confidence bounds reveal
 18 a slight positive TEC trend for the period 1999-2017. For the period 2003-2017, the trend
 19 estimates from the three data sets show that TEC trends over MAL2 are positive. To study
 20 the trends in TEC over the African low latitude region, we used the GIMs and estimated the
 21 trends in each of the $2.5^\circ \times 5^\circ$ (latitude \times longitude) grids. The trends are shown in Figure 10(a)
 22 and (c) for the period 1999-2017 and in Figure 10(b) and (d) for the period 2003-2017. The
 23 trends in Figure 10 show a latitudinal dependence with the trends in the vicinity of the crest
 24 of the EIA region being more positive than those near the magnetic equator, where the trend
 25 was negative over most of the African equatorial region. Analysis of the data from 1999-2017
 26

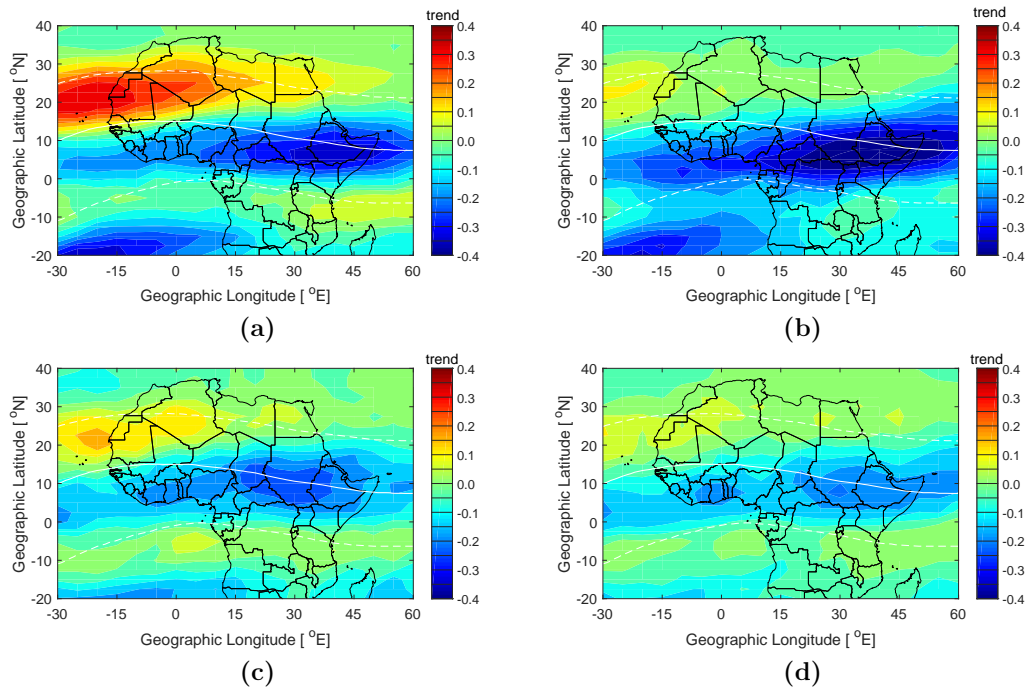


Figure 10: Trends in TEC over the African low latitude region derived from CODE's ((a) and (b)) and IGS's ((c) and (d)) GIMs. (a) and (c) are for the period 1999-2017 while (b) and (d) are for the period 2003-2017

1 revealed higher average value of TEC trends than that from 2003-2017 for both CODE's and
 2 IGS GIMs, though the general pattern of the trends remained unchanged. The trend pattern
 3 observed in this study confirm the latitudinal variation in TEC trends reported in Lean et al.
 4 (2011). The difference in the trend magnitudes for the periods 1999-2017 and 2003-2017 could
 5 be as pointed out earlier due to a bias towards lower values of GIMs prior to 2002 (Lastovicka
 6 et al., 2017; Emmert et al., 2017). If so, the trends in TEC over African low latitudes are
 7 therefore mainly negative, though cases of slight positive trends are also possible especially
 8 at the crest of the EIA region. Geomagnetic or anthropogenic factors are often the plausible
 9 physical mechanisms to explain trends in upper atmospheric parameters. The anthropogenic
 10 contributions to trends arises through the accumulation of greenhouse gases which result in
 11 decrease of atomic oxygen in the upper atmosphere. Some authors (e.g Danilov and Mikhailov
 12 1999; Mikhailov 2008) attribute the geomagnetic control of the trend to geomagnetic storms
 13 that result in compositions changes which in turn affect ionospheric currents. This latter view
 14 may explain the latitudinal dependence in the trends over African low latitude region.

15 6. Summary and Conclusion

16 We have used EOF expansion together with least square regression to model TEC over the
 17 African low latitude region. We first developed a single station model over MAL2, a station
 18 at the southern crest of the EIA, and then constructed a regional model to predict TEC over
 19 the African low latitudes. Despite the complicated nature of the low latitude ionosphere, the
 20 model over MAL2 was able to satisfactorily reproduce the diurnal, seasonal and solar activity
 21 variations in the observed TEC. Comparison of the model results with IRI-2016 derived TEC
 22 showed that the EOF-based TEC model was more accurate in predicting the daytime TEC over
 23 Malindi than IRI-2016. On the other hand, CODE's GIMs were better correlated with GPS



1 TEC than the TEC from the EOF-based model, though CODE's GIMs mainly overestimated
2 the GPS TEC over MAL2 during higher solar activity years. The large discrepancy of the
3 IRI-2016 predicted daytime TEC from the observed TEC over MAL2 during periods of low
4 solar activity and during the winter solstice could be due to over representation of the effects of
5 the low latitude $E \times B$ plasma drifts and thermospheric winds in the model. The regional model
6 reproduced quite well the known features of the low latitude ionosphere. Using the TEC from
7 the EOF-based model as background TEC to suppress solar and magnetic activity dependence
8 of TEC, we estimated trends in TEC over the African low latitude region. The regional trends
9 showed a latitudinal dependence with the trends in the vicinity of the magnetic equator being
10 more negative than those at the crest of the EIA.

11 Acknowledgement

12 This study was made possible by financial support from International Science Programme (ISP)
13 of Uppsala University in Sweden. We acknowledge the administration and staff of the Space
14 Science Directorate of the South African National Space Agency (SANSA) for the support
15 during the research visit of the first author to the institution.

16 References

- 17 Adewale, A. O., Oyeyemi, E. O., Adelaye, A. B., Ngwira, C. M., and Athieno, R.: Responses of
18 equatorial F region to different geomagnetic storms observed by GPS in the African sector,
19 J. Geophys. Res., 116, A12 319, 2011.
- 20 Anderson, D. N., Mendillo, M., and Herniter, B.: A semi-empirical low-latitude ionospheric
21 model, Radio Sci., 22, 292–306, 1987.
- 22 Andima, G., Jurua, E., Amabayo, E. B., and Habarulema, J. B.: Statistical analysis of TEC
23 perturbations over a low latitude region during 2009–2013 ascending solar activity phase,
24 Adv. Space Res., 56, 2542–2551, 2015.
- 25 Appleton, E. V.: Two Anomalies in the Ionosphere, Nature, 157, doi10.1038/157691a0, 1946.
- 26 Bencze, P.: Some results referring to the long-term change of ionospheric parameters, Acta
27 Geod. Geoph. Hung, 37, 403–408, 2002.
- 28 Bencze, P.: On the long-term change of ionospheric parameters, J. Atmos. Sol.-Terr., 67, 1298–
29 1306, 2005.
- 30 Bilitza D.: International reference ionosphere 1990. National Space Science Data Center, 1990
- 31 Bremer, J., Damboldt, T., Mielich, J., and Suessmann, P.: Comparing long-term trends in the
32 ionospheric F2-region with two different methods, J. Atmos. Sol.-Terr. Phys., 77, 174–185,
33 2012.
- 34 Chen, Z., Zhang, S.-R., Coster, A. J., and Fang, G.: EOF analysis and modeling of GPS TEC
35 climatology over North America, J. Geophys. Res.: Space Physics, 120, 3118–3129, 2015.
- 36 Danilov, A. D. and Mikhailov, A. V.: Spatial and seasonal variations of the foF2 long-term
37 trends, Ann. Geophys., 17, 1239–1243, 1999.
- 38 Dvinskikh, N. I.: Expansion of ionospheric characteristics fields in empirical orthogonal func-
39 tions, Adv. Space Res., 8, 179–187, 1988.



- 1 Elias, A. G.: Possible Sources of Long-Term Variations in the Mid-Latitude Ionosphere, J.
2 Open Atmos. Sci., 5, 9–15, 2011.
- 3 Emmert, J. T., Mannucci, A. J., McDonald, S. E., and Vergados, P.: Attribution of inter-
4 minimum changes in global and hemispheric total electron content, J. Geophys. Res. Space
5 Physics, 122, 2424–2439, 2017.
- 6 Ercha, A., Zhang, D., Ridley, A. J., Xiao, Z., and Hao, Y.: A global model: Empirical or-
7 thogonal function analysis of total electron content 1999–2009 data, J. Geophys. Res., 117,
8 A03328, 2012.
- 9 Habarulema, J. B., McKinnell, L.-A., Burešová, D., Zhang, Y., Seemala, G., Ngwira, C., Chum,
10 J., and Opperman, B.: A comparative study of TEC response for the African equatorial and
11 mid-latitudes during storm conditions, J. Atmos. Sol.-Terr. Phys., 102, 105–114, 2013.
- 12 Hajra, R., Chakraborty, S. K., Tsurutani, B. T., DasGupta, A., Echer, E., Gonzalez, C. G. B.
13 A. W. D., and Sobral, J. H. A.: An empirical model of ionospheric total electron content
14 (TEC) near the crest of the equatorial ionization anomaly (EIA), J. Space Weather Space
15 climate, 6, A29, 2016.
- 16 Hannachi, A., Jolliffe, I. T., and Stephenson, D. B.: Empirical orthogonal functions and related
17 techniques in atmospheric science: A review, Int. J. Climatol., 27, 1119–1152, 2007.
- 18 Hernandez-Pajares, M., Juan, J. M., Sanz, J., Orus, R., Garcia-Rigo, A., Feltens, J., Komjathy,
19 A., Schaer, S. C., and Krankowski, A.: The IGS VTEC maps: a reliable source of ionospheric
20 information since 1998, J. Geod., 83, 263–275, 2009.
- 21 Jarvis, M. J., Jenkins, B., and Rodgers, G. A.: Southern hemisphere observations of a long-
22 term decrease in F region altitude and thermospheric wind providing possible evidence for
23 global thermospheric cooling, J. Geophys. Res., 103, 20774–20787, 1998.
- 24 Kelley, M. C.: The Earth's ionosphere: Plasma Physics and Electrodynamics, Amsterdam,
25 academic Press, second edn., 2009.
- 26 Kersley, L., Malan, D., Pryse, S. E., Cander, L. R., Bamford, R. A., Belehaki, A., Leitinger, R.,
27 Radicella, S. M., Mitchell, C. N., and Spencer, P. S.: Total electron content-A key parameter
28 in propagation: measurement and use in ionospheric imaging, Ann. Geophys., 47, 1067–1091,
29 2004.
- 30 Lastovicka, J.: Are trends in total electron content (TEC) really positive, J. Geophys. Res.:
31 space physics, 118, 3831–3835, 2013.
- 32 Lastovicka, J., Mikhailov, A., Ulich, T., Bremer, J., Elias, A., de Adler, N. O., Jara, V., del Rio,
33 R. A., Foppiano, A., Ovalle, E., and Danilov, A.: Long-term trends in foF2: A comparison
34 of various methods, J. Atmos. Sol.-Terr. Phys., 68, 1854–1870, 2006.
- 35 Lastovicka, J., Urbar, J., and Kozubek, M.: Long-term trends in the total electron content, J.
36 Geophys. Res. Lett., 44, 8168–8172, doi10.1002/2017GL075063, 2017.
- 37 Lean, J. L., Emmert, J. T., Picone, J. M., and Meier, R. R.: Global and regional trends in
38 ionospheric total electron content, J. Geophys. Res., 116, A00H04, 2011.
- 39 Liu, C., Zhang, M.-L., Wan, W., Liu, L., and Ning, B.: Modeling M(3000)F2 based on empirical
40 orthogonal function analysis method, Radio Sci., 43, RS1003, 2008.



- 1 Martyn, D. F.: Atmospheric Tides in the Ionosphere. I. Solar Tides in the F₂ Region, Proc.
2 R. Soc. Lond., 189, 241–260, doi10.1098/rspa.1947.0037, 1947.
- 3 Mikhailov, A. V.: Ionospheric F1 layer long-term trends and the geomagnetic control concept,
4 Ann. Geophys., 26, 3793–3803, 2008.
- 5 Moffett, R. J.: The equatorial anomaly in the electron distribution of the terrestrial F-region,
6 Fund. Cos. Phy., 4, 313–391, 1979.
- 7 Olwendo, O., Cilliers, P., Baki, P., and Mito, C.: Using GPS-SCINDA observations to study
8 the correlation between scintillation, total electron content enhancement and depletions over
9 the Kenyan region, Adv. Space Res., 49, 1363–1372, 2012.
- 10 Opperman, B. D. L., Cilliers, P. J., McKinnell, L.-A., and Haggard, R.: Development of a
11 regional GPS-based ionospheric TEC model for South Africa, Adv. Space Res., 39, 808–815,
12 2007.
- 13 Pearson, K.: On lines and planes of closest fit to systems of points in space, Philos. Mag., 2,
14 559–572, 1901.
- 15 Rawer, K. and Bilitza, D.: International reference ionosphere-plasma densities: status 1988,
16 Adv. Space Res., 10, (8)5–(8)14, 1990.
- 17 Reinisch, B. W., Huang, X., Belehaki, A., Shi, J. K., Zhang, M. L., and R. Ilma: Modeling
18 the IRI topside profile using scale heights from ground-based ionosonde measurements, Adv.
19 Space Res., 34, 2026–2031, 2004.
- 20 Seemala, G. K. and Valladares, C.: Statistics of total electron content depletions ob-
21 served over the South American continent for the year 2008, Radio Sci., 46, RS5019,
22 doi:10.1029/2011RS004722, 2011.
- 23 Zhang, M. L., Liu, C., Wan, W., Liu, L., and Ning, B.: A global model of the ionospheric F2
24 peak height based on EOF analysis, Ann. Geophys., 27, 3203–3212, 2009.